Nanogap biosensors for electrical and label-free detection of biomolecular interactions

2009 Nanotechnology 20 455502

(http://iopscience.iop.org/0957-4484/20/45/455502)

Nanotechnology **20** (2009) 455502 (7pp) doi:10.1088/0957-4484/20/45/455502

Nanogap biosensors for electrical and label-free detection of biomolecular interactions

Sang Kyu Kim[1,2], Hyunmin Cho[1,2], Hye-Jung Park[1], Dohyoung Kwon[1], Jeong Min Lee[1] and Bong Hyun Chung[1,2,3]

[1] BioNanotechnology Research Center, Korea Research Institute of Bioscience and Biotechnology, PO Box 115, Yuseong, Daejeon 305-600, Republic of Korea
[2] Nanobiotechnology Major, School of Engineering, University of Science and Technology, PO Box 115, Yuseong, Daejeon 305-600, Republic of Korea

E-mail: chungbh@kribb.re.kr

Received 25 June 2009, in final form 11 September 2009
Published 13 October 2009
Online at stacks.iop.org/Nano/20/455502

Abstract
We demonstrate nanogap biosensors for electrical and label-free detection of biomolecular interactions. Parallel fabrication of nanometer distance gaps has been achieved using a silicon anisotropic wet etching technique on a silicon-on-insulator (SOI) wafer with a finely controllable silicon device layer. Since silicon anisotropic wet etching resulted in a trapezoid-shaped structure whose end became narrower during the etching, the nanogap structure was simply fabricated on the device layer of a SOI wafer. The nanogap devices were individually addressable and a gap size of less than 60 nm was obtained. We demonstrate that the nanogap biosensors can electrically detect biomolecular interactions such as biotin/streptavidin and antigen/antibody pairs. The nanogap devices show a current increase when the proteins are bound to the surface. The current increases proportionally depending upon the concentrations of the molecules in the range of 100 fg ml^{-1}–100 ng ml^{-1} at 1 V bias. It is expected that the nanogap developed here could be a highly sensitive biosensor platform for label-free detection of biomolecular interactions.

1. Introduction

The detection of an extremely low concentration of biomolecules such as DNA and protein is crucial for genomics [1], proteomics [2], and clinical diagnostics [3]. To obtain a high-sensitivity sensor, many researchers have developed various nanostructure-based biosensors with nanowires [4, 5], nanotubes [6, 7], microcantilevers [8], nanogaps [9, 10], and nanoparticles [11] because they provide remarkable capabilities for sensing extremely low concentrations of these molecules. In particular, nanogaps represent the simplest electronic structure, consisting of only one pair of electrodes with nanometer spacing. Nanogaps play very important roles in the fields of molecular electronics [12], sensors [13], and biological applications [14] due to the nanometer distance between the electrodes, providing an effective platform for surveying biomolecular interactions because the biomolecules inherently have similar nanometer dimensions.

Despite their superior features, it remains difficult to manufacture nanogap devices because conventional lithographic techniques mainly suffer from a light diffraction limitation. To overcome this limitation, nanogap structures have been fabricated using a variety of methods such as electron beam lithography [9], mechanical break junctions [15], electromigration [16], electrochemical deposition [17], thin film technology [10], and silicon-on-insulator wafers [18, 19]. Although these attempts have produced some outstanding outcomes, nanogap fabrication remains challenging because these methods still have disadvantages. For example, electron beam lithography, mechanical break junction, and electromigration methods are not suitable for high-throughput fabrication. Electrochemical deposition methods have difficulty in providing well-defined patterns and thin film technology requires relatively complex fabrication processes.

[3] Author to whom any correspondence should be addressed.

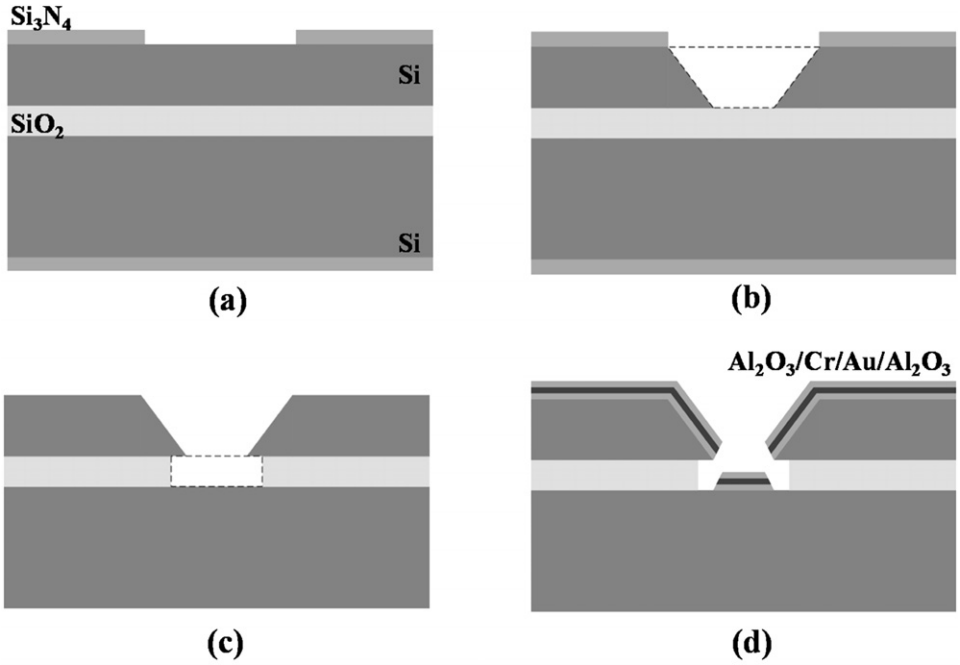

Figure 1. Schematic representation of the nanogap fabrication process. (a) The window patterns were defined by photolithography and reactive ion etching. (b) The trapezoid (dotted line) was created by anisotropic wet etching and a nano-size region was created at the buried oxide layer. (c) The silicon nanogap structure was formed after the masking layer and the buried oxide layer were removed by HF etching. (d) The nanogap device was completed by photolithography for the electrode after deposition of the insulator (Al_2O_3), metals (Cr/Au), and passivation layer (Al_2O_3).

One promising approach to solving these problems is the use of silicon anisotropic wet etching on a silicon-on-insulator (SOI) wafer. The silicon anisotropic wet etching process results in a V-groove or trapezoid-shape structure because etchants such as tetramethylammonium hydroxide (TMAH) and potassium hydroxide (KOH) etch the silicon (111) plane more slowly than the other planes [20]. The SOI wafer consists of a device layer and a buried oxide layer with a finely controllable nano-sized thickness on a handle layer. Therefore, some nanostructures, such as nanogaps and nanochannels, can be fabricated through anisotropic wet etching on the device layer of a SOI wafer using the feature of the etching process that reduces the size of the structure.

Here we describe a simple and cost-effective method for fabricating a well-defined nanogap between gold electrodes by silicon anisotropic wet etching on a SOI wafer device and its biological application to biosensors. The size of the nanogap was less than 60 nm and could be controlled by adjusting the initial window size and the thickness of the deposited materials. Using this nanogap, we implemented a nanogap biosensor to electrically detect biomolecular interactions of biotin/streptavidin and antigen/antibody without any labels. The receptor molecules were specifically bound to the electrode between the nanogap and electrical changes were detected due to the target proteins. The nanogap sensor presented here does not require either signal indicators or enhancing molecules and could be useful for point-of-care diagnostics and medicine.

2. Experimental details

2.1. Fabrication of nanogap device

The fabrications were carried out on boron-doped p-type (100) SOI wafers (IBIS Technology, USA) with an epitaxially grown 1 μm thick device layer. Starting from an optically defined line pattern on the micrometer scale, silicon anisotropic and silicon dioxide isotropic wet etching produced a gap a few tens of nanometers wide. Four types of initial window patterns (1.1, 1.2, 1.3, and 1.4 μm) were defined by optical lithography onto the SOI wafer with a 10 nm thick silicon nitride (Si_3N_4) layer that was grown by low pressure chemical vapor deposition (LPCVD). After reactive ion etching (RIE) removed the Si_3N_4 layer to expose the silicon, silicon anisotropic wet etching using 20 wt% KOH solution was performed for 75 s at 80 °C to achieve an inverse trapezoidal shape with the shorter side in contact with the buried oxide (SiO_2) layer (dotted line in figure 1(b)). Then the exposed oxide layer was removed by 49% hydrofluoric acid (HF) etching for 30 s. These processes created tapered silicon structures (silicon nanogap) that faced each other across a nanometer distance gap and formed a rectangular cavity in the buried oxide layer (dotted line in figure 1(c)). After the deposition of an insulating layer of Al_2O_3 (50 nm), the metal layers of Cr (1.5 nm) and Au (50 nm) were deposited for electrodes by an electron beam evaporator. Finally, a 10 μm wide electrode was defined by photolithography and then the surface was passivated with Al_2O_3 (60 nm) except for the contact pads, resulting in a nanogap biosensor device (figure 1(d)).

2.2. Surface modification for biological applications

After the gold surfaces of the nanogap devices were cleaned using acetone, methanol and then deionized water, oxygen plasma treatment (300 W) was performed for 120 s to make the surface hydrophilic, conferring wettability in the gap region. The gold surface was treated using 3 mM *N*-(6-(biotinamido)hexyl)-3′-(2′-pyridyldithio)-propionamide (biotin-HPDP, Pierce) in dimethyl sulfoxide (DMSO) solution for 1 h to form a biotinylated surface. To remove the unreacted molecules, the samples were washed several times with DMSO solution and PBS (phosphate buffer saline, pH 7.4) buffer. After immobilization of the biotin molecules on the gold surface, the device was incubated for 30 min at room temperature with streptavidin at 100 ng ml^{-1}. Before the electrical signal was measured, the nanogap devices were washed several times with PBS buffer to remove the unbound molecules.

After preparation of the nanogap device chip via the aforementioned process, a genetically engineered recombinant protein G tagged at the *N*-terminal by three cysteines (cys3–protein G) was used to capture an antibody on the solid support [21]. After a 100 μg ml^{-1} cys3–protein G molecule in PBS was immobilized on the gold surface for 30 min, 1 mg ml^{-1} bovine serum albumin (BSA) in PBS was incubated for 30 min to avoid non-specific interactions at the interface between gold and biomolecules. Subsequent PSA antibody was immobilized to cys3–protein G at a concentration of 10 μg ml^{-1} for 30 min. Intensive washing with PBS solution was undertaken at the end of each step to remove physically adsorbed molecules from the surface.

2.3. Electrical characterization

The current–voltage characteristic curve was obtained in PBS buffer solution from −1.0 to 1.0 V with a step of 0.02 V using a semiconductor characterization system (4200-SCS, Keithley) on a probe station.

3. Results and discussion

The process for fabricating the nanogap device is schematically illustrated in figure 1. The nanometer-size region was exposed on the buried oxide layer because the anisotropic wet etching produced a narrower end to the trapezoidal structure than that of the predefined pattern (figures 1(b) and 2(a)). This anisotropic trapezoidal structure was caused by silicon plane selectivity [20]. The subsequent HF etching process selectively removed the silicon oxide, resulting in a sharp-edge silicon nanogap structure with a rectangular cavity (figures 1(c) and 2(b)). The masking layer is not observed in figure 2(b) because the silicon nitride layer was removed by HF etching.

The final silicon nanogap sizes were 222 ± 23 nm, 166 ± 23 nm, and 58 ± 19 nm for initial window sizes (photomask pattern sizes) of 1.4 μm, 1.3 μm, and 1.2 μm, respectively. The error bars indicate the standard deviations for 34 devices. The nanogaps appeared for the three larger cases but not for the 1.1 μm case; the 1.1 μm window is too small to make a gap at the buried oxide region under the given conditions. The variation of the width along the gap was less than 10% in the electrode region. The estimated smallest gap width was 31 nm in the case of the 1.2 μm initial window. These results show that the dimension of the nanogap could be controlled by changing the window sizes.

Each nanogap sensing device comprises five individually addressable and electrically isolated electrodes ($<10^{-12}$ A at 1 V bias voltage, data not shown) with a lithographically defined 10 μm width. Figure 2(d) shows the well-defined stack of materials, which consist of insulators (Al_2O_3) and metals (Cr and Au) deposited by electron beam evaporation. Because the materials were evaporated under a high vacuum condition ($\sim10^{-6}$ Torr), the evaporated material particles had a long mean free path (>1 m), allowing the evaporated particles to travel directly to the target samples where they were again condensed to a solid state. The evaporated particles attacked the samples unidirectionally (poor step coverage); therefore, previously deposited materials could be exposed to the air (figures 2(e) and (f)). Transmission electron microscopy (TEM) analysis was also performed to confirm the formation of the deposited layers in detail. The cross-sectional image (figure 2(e)) shows the materials with well-defined boundaries in the order Al_2O_3/Cr/Au/Al_2O_3. The gap size was smaller than that obtained before the evaporation because the evaporation-deposited particles on the substrate had a tilted geometry, with an angle of 54.6°. The size of the nanogap could be further controlled by adjusting the thickness of the deposited materials.

To test whether the nanogap structure can be used as a biosensing platform, we first investigated the biomolecular interaction of biotin and streptavidin as a model system. The inset of figure 3 shows the change in electrical current when biotin interacted with a bare gold surface. No significant electric change was detected. This means that the biotin molecules did not contribute to current flow between the electrodes. The reason why the asymmetrical *I*–*V* curves appeared might be explained by a Schottky barrier, which is formed at a metal–semiconductor junction. Our system consists of two metallic electrodes on a silicon (semiconductor) substrate with a thin insulator (Al_2O_3). The asymmetrical current in our experiments might be caused by a Schottky barrier behavior, as in some related reports [22, 23]. The *I*–*V* curve shows finite currents at zero voltage. This might be caused by the charging effect on electrical double layer capacitance as similar result have been reported by Strobel *et al* [19]. We obtained the *I*–*V* curves by averaging over the forward and backward directions to cancel out bare charging effects. Figure 3(a) shows the change in electrical current when streptavidin interacted with biotin on the gold surface. This experiment was carried out with the ∼60 nm nanogap device. When streptavidin interacted with biotin, the intensity of the current signal increased from 2.8 nA to 5.0 nA and from −3.3 nA to −4.0 nA at 1 V and −1 V biases, respectively. These current changes are due to the binding event between biotin and streptavidin in the gold surface.

We also explored the dependence of the current intensity on gap size. When streptavidin interacted with biotin on the surface of the ∼140 nm nanogap device, the intensity of the

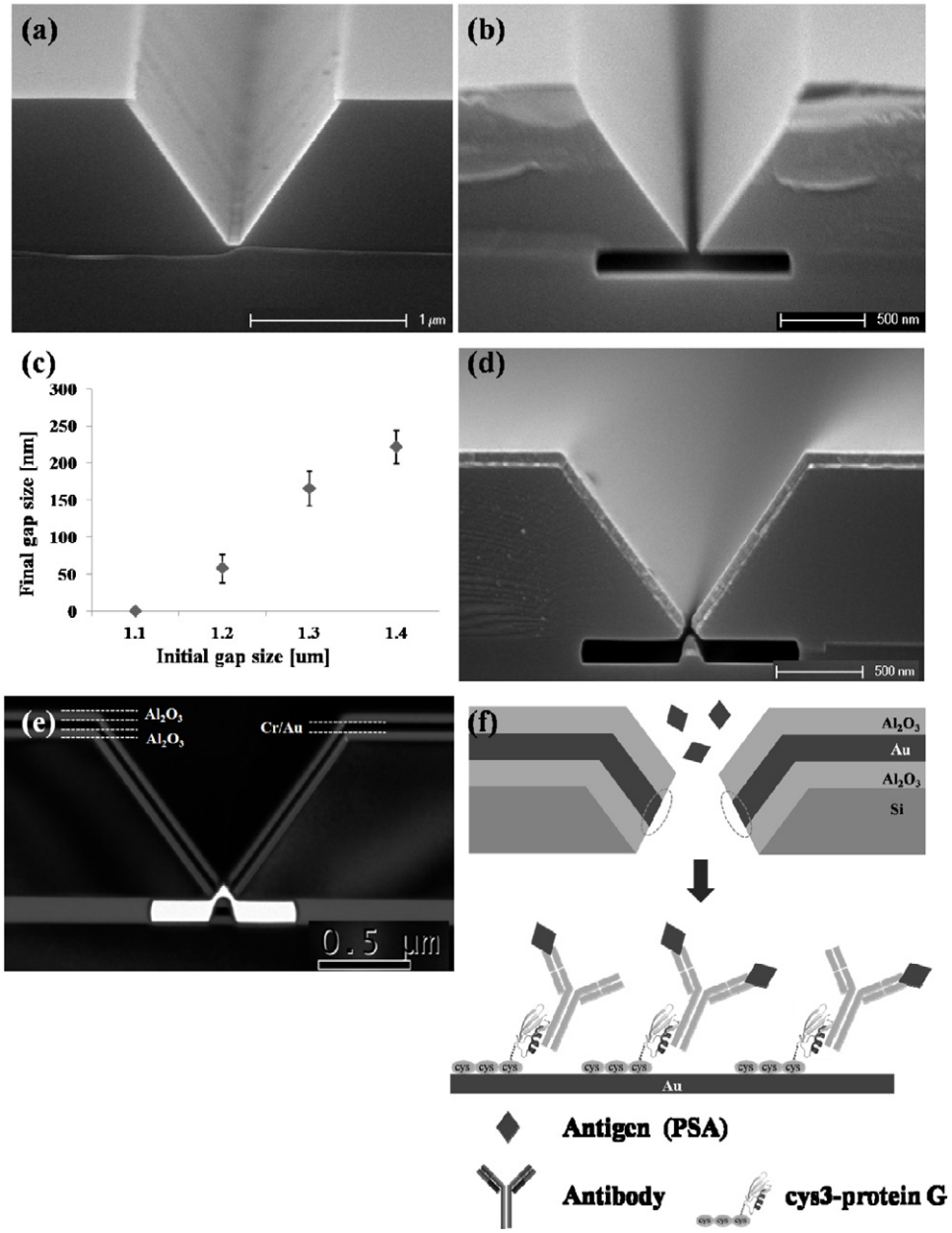

Figure 2. (a) Cross-sectional image of the trapezoid structure after silicon anisotropic wet etching. The buried oxide region with nano-size dimension is exposed. (b) The silicon nanogap was formed on the buried oxide layer after HF etching. Also shown is the rectangular cavity in the buried oxide layer. (c) Size distributions of the silicon nanogap according to the initial window size with error bars showing the standard deviation. The size of the nanogap was proportional to the initial window size. Nanogaps were obtained except for the 1.1 μm window, which is too narrow to create a nanogap. (d) The cross-sectional SEM image of the nanogap device after the insulation, metal, and passivation layers were deposited by the e-beam evaporation system, showing a well-defined stack of materials. (e) Cross-sectional TEM image for the nanogap device. Each layer of the nanogap device is clearly distinguished. The metal (Cr/Au) layers between the aluminum oxide layers are exposed, facing each other. (f) The scheme for the surface modification shows that the antigens (PSA) were detected after the antibodies were immobilized to the cys3–protein G-modified gold surface.

current signal increased from 2.4 nA to 2.7 nA and from −2.4 nA to −2.6 nA at 1 V and −1 V biases, respectively. The last shows a lower overall current intensity than that of the smaller gap device (figure 3(b)). We believe that this was caused by an increase in the potential drop in buffer between electrodes due to their greater separation distance. This result shows that the signal intensity of the nanogap device could be controlled by changing the gap size. A control experiment was performed by introducing 1 μg ml^{-1} streptavidin to the bare gold surface in the nanogap without biotin modification. No significant signal change was observed in the absence of biotin (not shown). This indicates that the streptavidin was specifically bound to the biotin surface.

A further investigation of biological interactions was performed with an immunoassay using monoclonal antibody [21] as a targeting moiety and prostate specific antigen (PSA) [24]

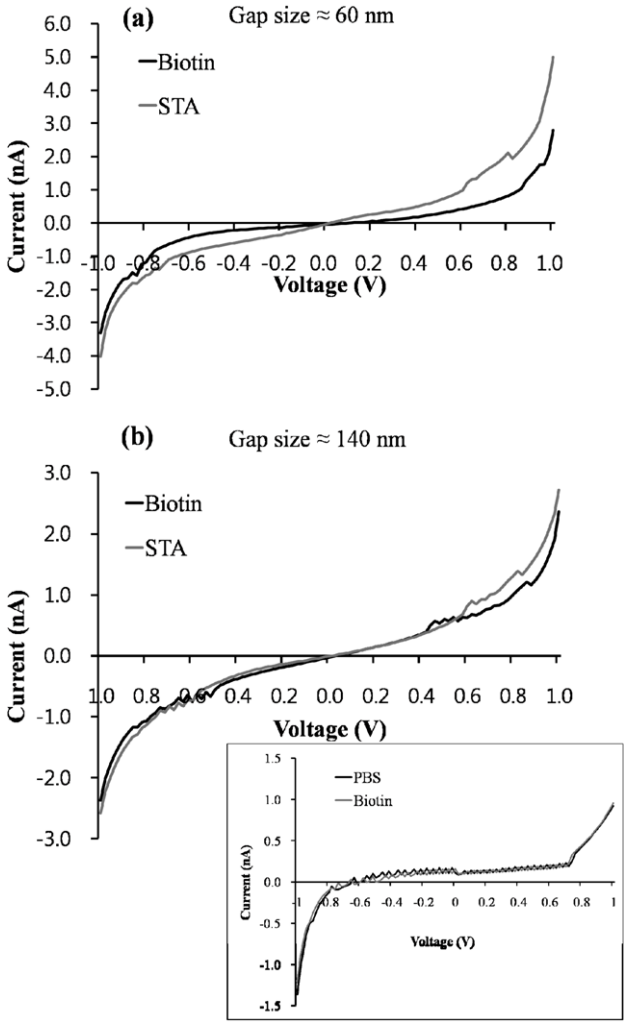

Figure 3. (a) I–V characteristic for the interaction between biotin and streptavidin (STA) on a ∼60 nm nanogap device. The current signal was increased after the streptavidin (gray line) bound to the biotinylated surface (black line). (b) I–V characteristic on a ∼140 nm nanogap device under the same conditions. The inset shows the current change after the biotin interacted with a bare gold surface.

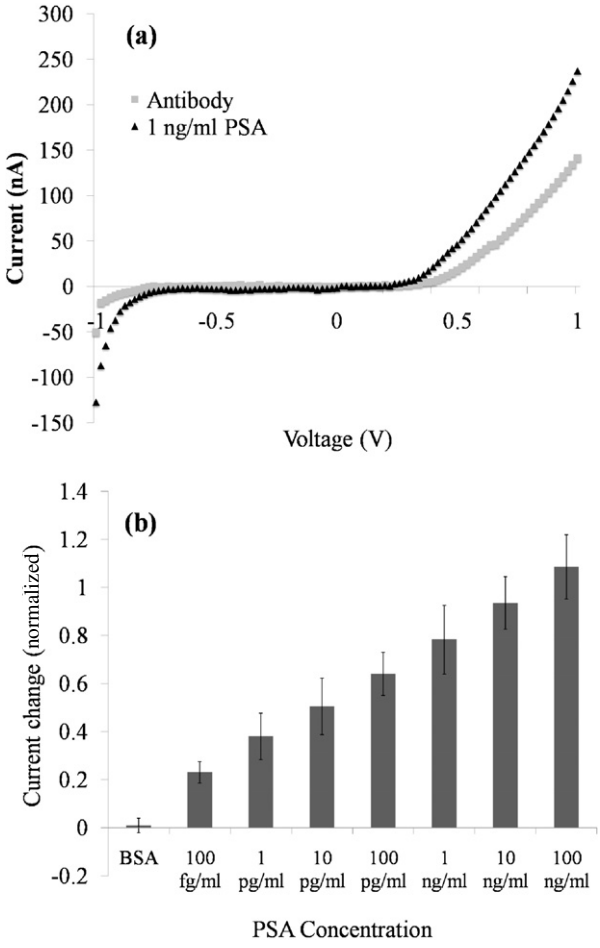

Figure 4. (a) I–V characteristic for the PSA antigen–antibody interaction and the signal increase when the antigen (black triangle) is bound to the antibody (gray rectangle). (b) Signal dependence on PSA concentration in terms of the normalized current change at 1 V. The signal change is proportional to the concentration of PSA within the range of 100 fg ml^{-1}–100 ng ml^{-1}. The error bars shows the relative standard deviations from nine devices.

as a target molecule on the ∼60 nm nanogap device. A schematic representation of the biologically modified surface is shown in figure 2(f). A genetically engineered recombinant protein G tagged at the *N*-terminal by three cysteines (cys3–protein G) was chosen as a good linker to immobilize the antibody on the gold support with a well-ordered orientation because the cysteine residue has a high affinity for gold and protein G is bound by the Fc region of an antibody molecule [21]. The current–voltage characteristics of the interaction between PSA antigen and antibody are shown in figure 4(a). The current signal increased from 141 to 238 nA at 1 V bias when 1 ng ml^{-1} PSA interacted with the antibody. No significant difference was detected between forward and backward scans. However, a little hysteresis was observed between both directions. Unfortunately, we could not obtain the curves depending on scan speed because our detecting system does not provide an option for arbitrarily controlling scan speed. We believe that the magnitude of the hysteresis depends on the scan speed as Strobel *et al* described [19].

We also investigated the signal dependence on protein concentrations. The average current values at 1 V as a function of the concentration of PSA are shown, with standard deviations, for nine devices in terms of the normalized relative change between the currents before and after PSA binding divided by the current before binding (figure 4(b)). The current change was directly proportional to the concentration of PSA in the range of 100 fg ml^{-1}–100 ng ml^{-1}. The results show that increasing the concentration of the target proteins causes the signal to increase. We also investigated the device selectivity in a competitive binding experiment with 1 mg ml^{-1} BSA. There was no significant signal change in such a high concentration of non-specific proteins.

These results cannot be exactly explained but we suppose two possible interpretations. One is an electrochemical reaction of the proteins on the gold surface. Due to the presence of charged proteins and ionic species in a buffer solution, the Faradaic current was generated by

an electrochemical process on the gold surface. The antibody–antigen interaction shows increased signal after PSA was bound to the antibody, probably due to the local electrochemical reaction of the proteins (PSA) on the gold surface. Because some amino acid residues such as tyrosine (Tyr) and tryptophan (Trp) are electro-active, proteins containing these residues contribute to the increase in electrical current [25]. Our results are in agreement with a previous report [25] on electrochemical detection of PSA. The electrochemical reaction on the gold surface seems to increase the electrical signal between the electrodes of the nanogap. Streptavidin also contains electro-active tyrosine and tryptophan residues [26], and therefore the binding event of streptavidin may also increase the electrical current signal.

Another interpretation of our results is conduction through a molecule–electrolyte–molecule junction between the nanogap electrodes. It is known that proteins have good electrical conductivity in an aqueous solution [27], and we could deduce from the previous reports [10, 28] that the protein in the buffer is more conductive than the buffer itself. When the proteins bind to the gold surface, more conductive proteins such as streptavidin and PSA are partially filled between nanogap electrodes. The electrical signal, therefore, will increase due to a reduction in the overall resistance between nanogap electrodes. Jang *et al* [28] showed a dramatic increase in current when the streptavidin bound to the biotin surface and formed a bridge between the nanogap (12 nm) electrodes, and the current increase of the device decreased as the gap size increased. While our results did not show a dramatic current increase because the gap is rather too large to be directly bridged by the proteins, we showed that the electrical signal was changed by the binding event and the concentration of the proteins. We obtained a current increase of 2.2 nA and 0.7 nA at 1 V and −1 V, respectively from the smaller gap (∼60 nm). We also obtained a current change of 0.3 nA and 0.2 nA at 1 V and −1 V, respectively, from a larger gap (∼140 nm). These results show that the smaller gap led to a higher current increase, agreeing with a previous report [28]. With these mechanisms, this nanogap device does not need any labeling materials, whereas previous experiments have used metal nanoparticles and enhancing materials to increase the signals [9].

We additionally tested the role of the passivation layer, which is critical in sensing biomolecular interactions. When the nanogap device was not passivated, a signal change was not detected (data not shown). The passivation process allowed blocking of the gold surface except for a small active region (figure 2(f)). If the region where the binding reactions occur is large, the signal change generated from the interactions between the biomolecules on the gold surface could be difficult to detect, because the current due to ions from the buffer solution and the resistance of the buffer would dominate. Thus, it seems that the passivation layer helps to increase the sensitivity.

In conclusion, we have demonstrated a new method for the simple fabrication of a nanogap using silicon anisotropic wet etching on a SOI structure. The inherent narrowing of the channel by the anisotropic wet etching to form a trapezoid allowed the fabrication of nanostructures without an e-beam facility. Because this method is based on optical lithography and a conventional micromachining technique, it is well suited for the production of well-defined structures on a large scale. We also succeeded in applying this method to electrically detect biological interactions such as biotin–streptavidin and antigen–antibody in the absence of any labeling process. The nanogap sensor could detect an extremely low concentration of 100 fg ml^{-1} PSA. We believe that this label-free nanogap sensor could be useful for clinical diagnostics, medicine, genomics, and proteomics.

Acknowledgments

This research was supported by a grant from the KRIBB Initiative Research Program (KRIBB, Korea) and the Fundamental R&D Program for Core Technology of Materials funded by the Ministry of Knowledge Economy, Republic of Korea (grant no: TGC 0300811).

References

[1] Janasek D, Franzke J and Manz A 2006 Scaling and the design of miniaturized chemical-analysis systems *Nature* **442** 374–80
[2] Jung S O, Ro H-S, Kho B H, Shin Y-B, Kim M G and Chung B H 2005 Surface plasmon resonance imaging-based protein arrays for high-throughput screening of protein-protein interaction inhibitors *Proteomics* **5** 4427–31
[3] Dawson E D, Moore C L, Dankbar D M, Mehlmann M, Townsend M B, Smagala J A, Smith C B, Cox N J, Kuchta R D and Rowlen K L 2007 Identification of A/H5N1 influenza viruses using a single gene diagnostic microarray *Anal. Chem.* **79** 378–84
[4] Zheng G, Patolsky F, Cui Y, Wang W U and Lieber C M 2005 Multiplexed electrical detection of cancer markers with nanowire sensor arrays *Nat. Biotechnol.* **23** 1294–301
[5] Stern E, Klemic J F, Routenberg D A, Wyrembak P N, Turner-Evans D B, Hamilton A D, LaVan D A, Fahmy T M and Reed M A 2007 Label-free immunodetection with CMOS-compatible semiconducting nanowires *Nature* **445** 519–22
[6] Star A, Gabriel J-C P, Bradley K and Gruner G 2003 Electronic detection of specific protein binding using nanotube FET devices *Nano Lett.* **3** 459–63
[7] So H-M, Won K, Kim Y H, Kim B-K, Ryu B H, Na P S, Kim H and Lee J-O 2005 Single-walled carbon nanotube biosensors using aptamers as molecular recognition elements *J. Am. Chem. Soc.* **127** 11906–7
[8] Wu G, Datar R H, Hansen K M, Thundat T, Cote R J and Majumdar A 2001 Bioassay of prostate-specific antigen (PSA) using microcantilevers *Nat. Biotechnol.* **19** 856–60
[9] Haguet V, Martin D, Marcon L, Heim T, Stievenard D, Olivier C, El-Mahdi O and Melnyk O 2004 Combined nanogap nanoparticles nanosensor for electrical detection of biomolecular interactions between polypeptides *Appl. Phys. Lett.* **84** 1213–5
[10] Im H, Huang X-J, Gu B and Choi Y-K 2007 A dielectric-modulated field-effect transistor for biosensing *Nat. Nanotechnol.* **2** 430–4
[11] Nam J-M, Thaxton C S and Mirkin C A 2003 Nanoparticle-based bio-bar codes for the ultrasensitive detection of proteins *Science* **301** 1884–6
[12] Nitzan A and Ratner M A 2003 Electron transport in molecular wire junctions *Science* **300** 1384–9

[13] Yi M, Jeong K-H and Lee L P 2005 Theoretical and experimental study towards a nanogap dielectric biosensor *Biosens. Bioelectron.* **20** 1320–6
[14] Yoo K H, Ha D H, Lee J O, Park J W, Kim J, Kim J J, Lee H Y, Kawai T and Choi H Y 2001 Electrical conduction through poly(dA)-poly(dT) and poly(dG)-poly(dC) DNA molecules *Phys. Rev. Lett.* **87** 198102
[15] Zhou C, Muller C J, Deshpande M R, Sleight J W and Reed M A 1995 Microfabrication of a mechanically controllable break junction in silicon *Appl. Phys. Lett.* **67** 1160–2
[16] Park H, Lim A K L, Alivisatos A P, Park J and McEuen P L 1999 Fabrication of metallic electrodes with nanometer separation by electromigration *Appl. Phys. Lett.* **75** 301–3
[17] Chen F, Qing Q, Ren L, Wu Z and Liu Z 2005 Electrochemical approach for fabricating nanogap electrodes with well controllable separation *Appl. Phys. Lett.* **86** 123105
[18] Berg J, Che F, Lundgren P, Enoksson P and Bengtsson S 2005 Electrical properties of Si–SiO_2–Si nanogaps *Nanotechnology* **16** 2197–202
[19] Strobel S, Arinaga K, Hansen A and Tornow M 2005 A silicon-on-insulator vertical nanogap device for electrical transport measurements in aqueous electrolyte solution *Nanotechnology* **18** 1983–5
[20] Jaeger R C 2001 *Introduction to Microelectronic Fabrication* (Englewood Cliffs, NJ: Prentice-Hall)
[21] Lee J M, Park H K, Jung Y, Kim J K, Jung S O and Chung B H 2007 Direct immobilization of protein G variants with various numbers of cysteine residues on a gold surface *Anal. Chem.* **79** 2680–7
[22] Tsai C, Chang T, Uppala R, Chen C, Ko F and Chen P 2005 Electrical detection of protein using gold nanoparticles and nanogap electrodes *Japan. J. Appl. Phys.* **44** 5711
[23] Chang T, Tsai C, Sun C, Chen C, Kuo L and Chen P 2007 Ultrasensitive electrical detection of protein using nanogap electrodes and nanoparticle-based DNA amplification *Biosens. Bioelectron.* **22** 3139–45
[24] Armbruster D 1993 Prostate-specific antigen: biochemistry, analytical methods, and clinical application *Clin. Chem.* **39** 181–95
[25] Okuno J, Maehashi K, Kerman K, Takamura Y, Matsumoto K and Tamiya E 2007 Label-free immunosensor for prostate-specific antigen based on single-walled carbon nanotube array-modified microelectrodes *Biosens. Bioelectron.* **22** 2377–81
[26] Argarana C E, Kuntz I D, Birken S, Axel R and Cantor C R 1986 Molecular cloning and nucleotide sequence of the streptavidin gene *Nucleic. Acids Res.* **14** 1871–82
[27] Rosenberg B 1962 Electrical conductivity of proteins *Nature* **193** 364–5
[28] Jang D-Y, Kim Y-P, Kim H-S, Park S-H K, Choi S-Y and Choi Y-K 2007 Sublithographic vertical gold nanogap for label-free electrical detection of protein–ligand binding *J. Vac. Sci. Technol.* B **25** 443–7